



This discussion paper is/has been under review for the journal Geoscientific Model Development (GMD). Please refer to the corresponding final paper in GMD if available.

The Joint UK Land Environment Simulator (JULES), Model description – Part 2: Carbon fluxes and vegetation

D. B. Clark¹, L. M. Mercado¹, S. Sitch², C. D. Jones³, N. Gedney⁴, M. J. Best³, M. Pryor⁴, G. G. Rooney³, R. L. H. Essery⁵, E. Blyth¹, O. Boucher³, R. J. Harding¹, and P. M. Cox⁶

¹Centre for Ecology and Hydrology, Wallingford, OX10 8BB, UK

²School of Geography, University of Leeds, Leeds LS2 9JT, UK

³Met Office Hadley Centre, Exeter, EX1 3PB, UK

⁴Met Office, Joint Centre for Hydro-Meteorological research, Wallingford, OX10 8BB, UK

⁵School of GeoSciences, University of Edinburgh, EH9 3JW, Edinburgh, UK

⁶College of Engineering, Mathematics and Physical Sciences, University of Exeter, Exeter, EX4 4QF, UK

Received: 2 March 2011 – Accepted: 4 March 2011 – Published: 24 March 2011

Correspondence to: D. B. Clark (dbcl@ceh.ac.uk)

Published by Copernicus Publications on behalf of the European Geosciences Union.

641

Abstract

The Joint UK Land Environment Simulator (JULES) is a process-based model that simulates the fluxes of carbon, water, energy and momentum between the land surface and the atmosphere. Past studies with JULES have demonstrated the important role of the land surface in the Earth System. Different versions of JULES have been employed to quantify the effects on the land carbon sink of separately changing atmospheric aerosols and tropospheric ozone, and the response of methane emissions from wetlands to climate change. There was a need to consolidate these and other advances into a single model code so as to be able to study interactions in a consistent manner. This paper describes the consolidation of these advances into the modelling of carbon fluxes and stores, in the vegetation and soil, in version 2.2 of JULES. Features include a multi-layer canopy scheme for light interception, including a sunfleck penetration scheme, a coupled scheme of leaf photosynthesis and stomatal conductance, representation of the effects of ozone on leaf physiology, and a description of methane emissions from wetlands. JULES represents the carbon allocation, growth and population dynamics of five plant functional types. The turnover of carbon from living plant tissues is fed into a 4-pool soil carbon model. The process-based descriptions of key ecological processes and trace gas fluxes in JULES mean that this community model is well-suited for use in carbon cycle, climate change and impacts studies, either in standalone mode or as the land component of a coupled Earth system model.

1 Introduction

Terrestrial ecosystems play an important role in land surface energy and trace gas exchange with the atmosphere. They currently absorb almost one third of the anthropogenic carbon dioxide emissions (Prentice et al., 2001; Le Quéré et al., 2009), although the locations and mechanisms for these terrestrial carbon sinks are debated and uncertain (Ciais et al., 1995; McGuire et al., 2001; Stephens et al., 2007; Phillips

642

et al., 2009). Furthermore, land-atmosphere exchange of non-CO₂ greenhouse gases, such as CH₄, O₃, and N₂O, affect atmospheric chemistry and climate (Arneeth et al., 2010). Vegetation and soils also exert a strong control on the surface energy balance and the physical state of the atmosphere. Anthropogenic climate change has been projected to radically alter the structure and function of terrestrial ecosystems (Cramer et al., 2001; Sitch et al., 2008). Future shifts in vegetation, such as a northward migration of the boreal forest into tundra, are likely to impact the climate via both biogeophysical and biogeochemical feedbacks. This spurred the development of Dynamic Global Vegetation Models (DGVMs; Cox, 2001; Sitch et al., 2003; Prentice et al., 2007) which describe the structure and function of the major global terrestrial ecosystems.

Advances in recent years have seen the inclusion in land surface models of first a carbon cycle (Cox et al., 2000) and a nitrogen cycle (Thornton et al., 2007; Sokolov et al., 2008). Using the TRIFFID DGVM coupled to a General Circulation Model (HadCM3LC), Cox et al. (2000) were the first to show the possibility of a positive climate-land carbon cycle feedback, through the counteracting effects of climate and atmospheric CO₂ on ecosystem function. A reduction in terrestrial carbon in response to climate change, leads to higher atmospheric CO₂ levels, and thus accelerated climate change. This has major policy implications for climate change mitigation (Jones et al., 2006). Friedlingstein et al. (2006) extended this work using 11 coupled climate-carbon cycle models. All models simulated a positive land carbon cycle feedback but of widely varying strengths and there was little consensus among models on the underlying mechanisms.

The land surface scheme used by Cox et al. (2000) was the Met Office Surface Exchange Scheme (MOSES; Cox et al., 1999; Essery et al., 2003). The representation of plant and soil processes in this model, and the implications for the modelled carbon cycle, have been the subject of several subsequent studies. In Cox et al. (2000) the positive feedback is attributed to enhanced soil decomposition in mid-latitudes with warming, and drought induced forest dieback across Amazonia (Betts et al., 2004; Cox et al., 2004). Subsequent studies investigated the structural uncertainty in future projections

643

associated with the soil carbon representation (Jones et al., 2005), the role of tropical ecosystems in the control of atmospheric CO₂ on the interannual timescales (Jones et al., 2003), and evaluated the coupled model against atmospheric data, proposing a prototype benchmarking methodology for coupled climate-carbon cycle models (Cadule et al., 2010). Jones et al. (2005) replaced the one-pool soil decomposition model with the more elaborate 4-pool model of RothC (Jenkinson, 1990; Coleman and Jenkinson, 1999) and concluded that the projection of a positive feedback between climate and carbon cycle is robust, however, the magnitude of the feedback is dependent on the structure of the soil carbon model. The multi-pool carbon dynamics of RothC cause it to exhibit a slower magnitude of transient response to both increased organic carbon inputs and changes in climate compared with the one-pool model.

Gedney et al. (2004) developed an interactive wetlands scheme model that was calibrated using present-day atmospheric CH₄ variability. They predicted increases in global CH₄ flux between present day and 2100 of 75% with an increase in emissions from northern wetlands (> 30° N) of 100%, despite an estimated 10% reduction in wetland extent. This wetland response corresponds to an amplification of the total anthropogenic radiative forcing at 2100 by 3.55%.

Sitch et al. (2007) showed how elevated future tropospheric O₃ concentrations would have detrimental effects on plant productivity, and reduce the efficiency of the terrestrial biosphere to sequester carbon, constituting a large indirect radiative forcing of tropospheric O₃ on climate. Mercado et al. (2009) showed how changes in surface irradiance over the global dimming and subsequent brightening period, 1960–2000, associated with changes in anthropogenic scattering aerosols and cloud cover, led to enhanced global plant productivity and carbon storage. Scattering aerosols change both the quantity and quality (diffuse component) of surface irradiance. Diffuse light is able to penetrate further into the canopy than direct light, stimulating production in light-limited understorey leaves. Mercado et al. (2009) found this diffuse radiation fertilisation effect was larger than the negative effect of reduced irradiance on global plant production. However Mercado et al. (2009) also showed local site optima in the

644

relationship between photosynthesis and diffuse light conditions; under heavily polluted or dark cloudy skies, plant productivity will decline as the diffuse effect is insufficient to offset decreased surface irradiance.

5 A comprehensive understanding and description of key ecological processes and nutrient cycles is needed in Earth system models. These include the cycles of carbon, nitrogen and phosphorus; the ecophysiological response of vegetation to changes in atmospheric composition (e.g. plant response to elevated CO₂ and O₃, N deposition, aerosol radiation effects); the response of vegetation and soils to drought and elevated temperatures; wetland processes and methane exchange; permafrost; and wildfire
10 disturbance. Currently, no single land surface model adequately describes all these processes.

This paper describes modelling of carbon fluxes and stores, in the vegetation and soil, as represented in version 2.2 of the Joint UK Land Environment Simulator (JULES). JULES was based on MOSES and consolidates the improved representations of key processes gained from the studies summarised in the preceding paragraphs. A companion paper (Best et al., 2011, hereafter referred to as Part 1) describes how JULES models fluxes of heat and moisture. Although they are presented separately, the fluxes of moisture and carbon are intimately linked, in particular through the stomatal resistance of the vegetation. The performance of JULES is assessed in
15 Blyth et al. (2010).

Section 2 provides a brief overview of JULES before Sect. 3 describes the photosynthesis model, which has been substantially augmented since Cox et al. (1999) with the addition of an explicit description of light interception at different canopy-levels which leads to a multi-layer approach to scaling photosynthesis from leaf to canopy scale.
20 The parameterisations of plant respiration and the effect of ozone on leaf photosynthesis are also covered in that section. The phenology model described in Sect. 4 is essentially unchanged since Cox et al. (1999). Section 5 outlines the simulation of soil carbon, which has changed with the introduction of a 4-pool model and the possibility of choosing between alternative descriptions of the response of heterotrophic respiration

645

to soil temperature. A parameterisation of methane emissions from wetlands is also outlined. Finally Sect. 6 gives details of the dynamic vegetation model, TRIFFID (Cox, 2001).

2 Model description

5 JULES describes the vegetation in a gridbox using a small number of Plant Functional Types (PFTs). The default is to use 5 PFTs: broadleaf trees, needleleaf trees, C₃ (temperate) grasses, C₄ (tropical) grasses and shrubs. The surface fluxes of CO₂ associated with photosynthesis and plant respiration are calculated in the physiology component of JULES, as described in Sect. 3 on each JULES timestep (typically 30
10 to 60 min). The accumulated carbon fluxes are passed to the vegetation dynamics model (TRIFFID, described in Sect. 6) and the area covered by each PFT is updated on a longer timestep (typically 10 days) based on the net carbon available to it and on the competition with other vegetation types, which is modelled using a Lotka-Volterra approach (Cox, 2001). Leaf phenology (bud-burst and leaf drop) is updated on an intermediate timescale of 1 day, using accumulated temperature-dependent leaf turnover rates (Sect. 4). Litterfall from vegetation is input to a model of soil carbon (Sect. 5) which calculates the rate of microbial soil respiration and the consequent flux of CO₂ back to the atmosphere. This part of the model has changed since Cox et al. (1999) with the introduction of a 4-pool model and the possibility of choosing between alternative descriptions of the response of heterotrophic respiration to soil temperature.
15 Methane emissions from wetlands are also calculated. After each call to TRIFFID the land surface parameters required by JULES (e.g. albedo, roughness length) are updated based on the new vegetation state, so that changes in the biophysical properties of the land surface, as well as changes in terrestrial carbon, may feed back onto the atmosphere. The land surface parameters are calculated as a function of the type,
20 height and leaf area index of the vegetation, as described in Sect. 6.2.

646

The net (unstressed by water availability) leaf photosynthetic carbon uptake, A_p , is calculated by subtracting the leaf dark respiration (R_d) from the gross photosynthetic rate, W :

$$W = \min(W_c, W_l, W_e) \quad (7)$$

$$R_d = f_d V_{cmax} \quad (8)$$

$$A_p = W - R_d \quad (9)$$

where f_d is the dark respiration coefficient.

Leaf photosynthesis is linked to stomatal conductance via the internal CO_2 concentration, which is calculated using the Jacobs (1994) formulation. The Jacobs formulation shares similarities with the stomatal conductance formulations of Ball et al. (1987) and Leuning (1995). A description of the coupled stomatal conductance-photosynthesis model is given in Part 1 and originally in Cox et al. (1998, 1999).

To account for soil moisture stress, the potential (non-stressed) leaf photosynthesis A_p is multiplied by a soil water factor (Cox et al., 1998):

$$A_l = A_p \beta \quad (10)$$

where A_l is leaf-level photosynthesis. β is the moisture stress factor (unit-less) which is related to the mean soil moisture concentration in the root zone, θ , and the critical and wilting point concentrations, θ_c and θ_w respectively, as follows:

$$\beta = \begin{cases} 1 & \text{for } \theta > \theta_c \\ \frac{\theta - \theta_w}{\theta_c - \theta_w} & \text{for } \theta_w < \theta \leq \theta_c \\ 0 & \text{for } \theta \leq \theta_w \end{cases} \quad (11)$$

3.2 Scaling photosynthesis from leaf to canopy

The description of within-canopy radiation interception and scaling from leaf to canopy-level photosynthesis has been developed considerably since Cox et al. (1999). JULES2.2 includes a process-based scaling-up of leaf-level photosynthesis to the canopy level, with alternative methods to calculate canopy radiation interception and canopy-level photosynthesis. There are two options available in JULES for scaling up from the leaf-level to the canopy scale: (i) the canopy is considered as a big leaf and (ii) a multi-layer canopy. Within the multi-layer option, JULES has four variations that depend on considerations of vertical gradients of canopy photosynthetic capacity, inclusion of light inhibition of leaf respiration, inclusion of sunfleck penetration and splitting canopy layers into sunlit and shaded leaves. All options are described below and summarised in Table 2.

3.2.1 Big leaf approach

Radiation interception and scaling up to canopy-level

In the big leaf approach, incident radiation attenuates through the canopy following Beer's law (Monsi and Saeki, 1953)

$$I_c = I_o e^{-kL_c} \quad (12)$$

where I_c is irradiance beneath the canopy, I_o irradiance at the top of the canopy, L_c is the canopy leaf area index and k is a light extinction coefficient.

Leaf-level photosynthetic capacity is assumed to vary proportionally with the vertical distribution of irradiance (Sellers et al., 1992), therefore leaf photosynthesis A_l can also be expressed as a function of the top of the canopy leaf photosynthesis A_o , leaf area index L and the light extinction coefficient:

$$A_l = A_o e^{-kL} \quad (13)$$

Canopy photosynthesis is calculated as the integral of leaf-level photosynthesis over the entire canopy leaf area index:

$$A_c = \int_0^{L_c} A_l dL = A_o \left[1 - e^{-kL_c} \right] / k \quad (14)$$

Canopy-level conductance and respiration are estimated using similar expressions.

5 3.2.2 Multi-layer approach

Radiation interception

The canopy is divided into a number of layers (n , typically 10) of equal leaf area increments $dL_c = L_c/n$. JULES adopts the two-stream approximation of radiation interception from Sellers (1985) to calculate surface spectral albedos (Essery et al., 2001) and the absorbed incoming radiation for each canopy layer. The absorbed incident PAR at each layer varies with solar zenith angle, incident direct and diffuse radiation at the top of the canopy, canopy leaf angle distribution and leaf radiation properties in the visible and near-infrared wavebands. JULES explicitly describes absorption and scattering of both direct and diffuse radiation fluxes separately in the visible and near-infrared wavebands at each canopy layer, which leads to the calculation of upward and downward diffuse fluxes of scattered direct beam radiation ($I_{dir \uparrow i}$, $I_{dir \downarrow i}$) and incident diffuse radiation and scattered diffuse radiation ($I_{dif \uparrow i}$, $I_{dif \downarrow i}$) per canopy layer. These fluxes are then used to calculate the direct and diffuse fractions of absorbed incident PAR, $FAPAR_{DIR_i}$ and $FAPAR_{DIF_i}$, at each canopy layer i :

$$FAPAR_{DIR_i} = [I_{dir \uparrow i} - I_{dir \downarrow i}] dL_c \quad (15)$$

$$FAPAR_{DIF_i} = [I_{dif \uparrow i} - I_{dif \downarrow i}] dL_c \quad (16)$$

A comparison of the vertical profile of absorbed incident PAR calculated with the two-stream approach against the profile estimated with Beer's law showed that the results

651

were similar only when the incident PAR was a direct beam coming from a high sun angle, otherwise the fraction of absorbed PAR at any canopy-level is higher when calculated using Beer's law (Jogireddy et al., 2006).

The two-stream approach provides a vertical profile of intercepted radiation within the canopy which allows estimation of photosynthesis and leaf respiration for each leaf area increment within the canopy.

Sunfleck penetration

A further improvement to the estimation of absorbed radiation fluxes within the canopy considers penetration of sunflecks through the canopy, which corresponds to the direct component of the direct beam radiation I_b , i.e. it excludes the scattering component. Such a term is not included in Eq. (15). Thus, attenuation of non-scattered incident beam radiation per unit leaf area at canopy depth L is (Dai et al., 2004):

$$I_b = I_{b_0} (1 - \omega) k_b \exp^{-k_b L} \quad (17)$$

where I_{b_0} is incident direct radiation, $(1 - \omega)$, is the non-scattered part of the incident beam (i.e. what is absorbed) and k_b is the canopy beam radiation extinction coefficient.

Following Dai et al. (2004) as implemented in Mercado et al. (2009), radiation fluxes are split into direct beam radiation, scattered direct beam and diffuse radiation and it is assumed that sunlit leaves absorb all types of radiation, while shaded leaves absorb only diffuse radiation. The fraction of sunlit leaves (f_{sun}), is defined as:

$$f_{sun} = \exp^{-k_b L} \quad (18)$$

For each canopy layer i with leaf area increment within the canopy (dL_c), the fraction of sunlit leaves, absorbed direct beam radiation (I_{b_i}), scattered direct beam (I_{bs_i}) and diffuse radiation (I_{d_i}) is calculated as:

$$f_{sun_i} = \frac{\exp^{-k_b L} (\exp^{-k_b d_c} - 1)}{k_b dL_c} \quad (19)$$

652

$$I_{b_i} = (1 - \omega) \left(\frac{\exp^{-k_b(L-dL_c)} - \exp^{-k_b L}}{dL_c} \right) \quad (20)$$

$$I_{bs_i} = \omega \left(\frac{\exp^{-k_b(L-dL_c)} - \exp^{-k_b L}}{dL_c} \right) + \text{FAPAR}_{\text{DIR}_i} \quad (21)$$

$$I_{d_i} = \text{FAPAR}_{\text{DIF}_i} \quad (22)$$

The fraction of radiation absorbed by sunlit leaves I_{sun_i} and shaded leaves I_{sh_i} at each leaf area increment within the canopy is calculated as:

$$I_{\text{sh}_i} = f_d I_{d_i} + (1 - f_d) I_{bs_i} \quad (23)$$

$$I_{\text{sun}_i} = I_{\text{sh}_i} + (1 - f_d) I_{b_i} / f_{\text{sun}_i} \quad (24)$$

where f_d is the fraction of PAR which is diffuse radiation. I_{sun_i} and I_{sh_i} are used to estimate photosynthesis from sunlit A_{sun_i} and shaded leaves A_{sh_i} for each leaf area increment within the canopy.

Scaling up to canopy-level

Canopy-scale fluxes are estimated as the sum of the leaf-level fluxes in each layer scaled by leaf area. Hence canopy-level photosynthesis is estimated from layer leaf-level photosynthesis (A_{i_j}) as follows:

$$A_j = A_{i_j} dL_c \quad (25)$$

$$A_c = \sum_{i=0}^n A_i \quad (26)$$

with A_i as photosynthesis from each canopy layer. When including sunflecks and accounting explicitly for photosynthesis by sunlit and shaded leaves, A_i is calculated as

$$A_i = f_{\text{sun}_i} A_{\text{sun}_i} + (1 - f_{\text{sun}_i}) A_{\text{sh}_i} \quad (27)$$

Canopy respiration and conductance are estimated in a similar manner.

653

Photosynthetic capacity at each canopy layer

The multi-layer scheme has been applied and tested against eddy correlation flux measurements (Mercado et al., 2007) using different assumptions of the vertical distribution of leaf nitrogen. Such a distribution is a proxy for the vertical distributions of photosynthetic capacity V_{cmax} and leaf respiration through the canopy. The distributions tested were a uniform distribution with leaf N constant through the canopy, and a distribution with leaf N decreasing from top to bottom of the canopy. In the latter case, the vertical profiles of leaf N, photosynthetic capacity and leaf respiration within the canopy were estimated following de Pury and Farquhar (1997) using measured vertical profiles from a rainforest site in the Amazon Basin (Carswell et al., 2000) and prescribed in JULES to decrease exponentially with increasing canopy depth (Mercado et al., 2007).

Photosynthetic capacity (V_{cmax_i}) at each canopy layer i is estimated as

$$V_{\text{cmax}_i} = N_0 n_e \exp^{-k_n i / n} \quad (28)$$

with N_0 the leaf N concentration at the top of the canopy and k_n a nitrogen allocation coefficient estimated to be 0.78. n_e is a constant that linearly relates leaf N concentration to Rubisco carboxylation capacity, with values of 0.0008 and 0.0004 for C_3 and C_4 plants, respectively. These values were derived from Schulze et al. (1994) assuming that 40 percent of the total leaf carbon mass is dry matter and that maximum rate of photosynthetic uptake is half of maximum photosynthetic capacity (Cox, 2001). Vertical profiles of V_{cmax} remain to be tested further and evaluated for other vegetation types.

An additional process is included in the multi-layer version of JULES which accounts for inhibition of leaf respiration in the light. Mercado et al. (2007) tested the inclusion of inhibition of leaf respiration by the light from Brooks and Farquhar (1985) as implemented by Lloyd et al. (1995) for a rainforest site in the Amazon. Once JULES was correctly parameterised for canopy photosynthetic capacity at this site, the inclusion of this inhibition allowed much better predictions of observed rates of net photosynthetic uptake.

654

3.2.3 Assessment of big-leaf and multi-layer approaches

JULES was evaluated using the multi-layer approach and eddy correlation data for a temperate coniferous forest site in the Netherlands (Jogireddy et al., 2006) and a tropical broad leaf rainforest site in the Brazilian Amazon (Mercado et al., 2007). Both studies demonstrated the superior performance of the multi-layer approach with the two-stream canopy radiation interception (Sellers, 1985) compared to the big-leaf approach in simulating canopy scale photosynthetic fluxes, specifically both the simulated light response and diurnal cycles of photosynthesis. Further evaluation of the multi-layer approach at eddy correlation sites and globally is presented in Blyth et al. (2010).

The multi-layer approach has been applied using different assumptions for the number of canopy layers (either 2 or 10). Jogireddy et al. (2006) compared simulated canopy photosynthesis using two and ten layers at a coniferous forest site, and found the 2-layer option to give a good fit to the 10-layer simulation. Because the two layer option is computationally efficient, Jogireddy et al. (2006) recommended this option for large scale applications if computer resources are limited. Allowing leaf nitrogen, canopy photosynthetic capacity and leaf respiration to vary through the canopy, provides a more realistic representation of canopy and total plant respiration in JULES; the description of stem and root respiration in JULES is a dependent function of canopy respiration and their respective nitrogen contents. This is especially apparent in tropical ecosystems, where simulations which assume a uniform vertical distribution of leaf N, and therefore photosynthetic capacity, produce very large respiration fluxes from leaves in the shaded understorey. Observations of a decrease of leaf N and photosynthetic capacity within canopies (Meir et al., 2002) and decrease of leaf respiration in the light (Brooks and Farquhar, 1985; Atkin et al., 1998; Hoefnagel et al., 1998; Atkin et al., 2000) support their inclusion into JULES.

Use of the two-stream canopy radiation interception scheme and multi-layer approach to photosynthesis provides realistic representation of the light response of

655

photosynthesis and its diurnal cycle, and having a non-uniform distribution of canopy photosynthetic capacity produces more realistic estimates of canopy and plant respiration. Also the scheme allows differentiation between direct and diffuse radiation, which is not possible using the Beer's law approach. Figure 1 shows evaluation of Gross Primary Productivity (GPP) simulated by JULES using eddy correlation data from a temperate broad leaf (Knohl et al., 2003) and a needle leaf (Rebmann et al., 2010) site. Observations are compared against JULES using the big leaf approach and the multi-layer option that includes vertical decrease of photosynthetic capacity and inclusion of light inhibition of leaf respiration (options 1 and 4 in Table 2). The multi-layer approach shows a more realistic light response and diurnal cycle of photosynthesis than the big leaf approach.

Inclusion of sun fleck provided a platform to study the differential effects of direct and diffuse radiation on carbon and water exchange. A global model application of the effects of diffuse radiation on the land carbon sink (Mercado et al., 2009) uses ten canopy layers and non-uniform distribution of photosynthetic capacity through the canopy. The 10-layer model, including sunfleck penetration, the vertical decrease in photosynthetic capacity within the canopy and the inhibition of respiration in the light, is the recommended default setting (option 5 Table 2) for applications at all scales from individual sites to global modelling. This is because it provides the most realistic representation of plant physiological processes. However, the inclusion of a vertical profile of photosynthetic capacity through the canopy is likely to require specific parameterisations for each PFT. In addition, the percentage inhibition of leaf respiration in the light is based on limited data for a small number of species. More observational data are needed to refine this inhibition and how it varies across plant functional types. These will be the focus of future model development.

3.3 Ozone effects on photosynthesis

Ozone causes cellular damage inside leaves which adversely affects plant production, reduces photosynthetic rates and requires increased resource allocation to detoxify

656

and repair leaves (Ashmore, 2005). JULES uses a flux-gradient approach to model ozone damage, following Sitch et al. (2007). It is assumed that ozone suppresses the potential net leaf photosynthesis in proportion to the ozone flux through stomata above a specified critical ozone deposition flux, so that the actual net photosynthesis (A) is given by

$$A = A_p F \quad (29)$$

where the reduction factor

$$F = 1 - a \max[F_{O_3} - F_{O_3 \text{ crit}}, 0] \quad (30)$$

is given by the instantaneous leaf uptake of O_3 over a plant type-specific threshold, $F_{O_3 \text{ crit}}$, in $\text{nmol m}^{-2} \text{s}^{-1}$, multiplied by a plant-specific parameter (a), following Pleijel et al. (2004). The cumulative effect of leaf damage and early senescence is implicitly accounted for in our calibration of a (by compensating a shortened growing season by reducing photosynthesis).

The flux F_{O_3} is calculated by analogy with Ohm's law as

$$F_{O_3} = \frac{[O_3]}{r_a + \kappa_{O_3}/g_l} \quad (31)$$

where $[O_3]$ is the molar concentration of O_3 at reference level (nmol m^{-3}), r_a is the aerodynamic and boundary layer resistance between leaf surface and reference level (s m^{-1}), g_l is the leaf conductance for H_2O (m s^{-1}), and $\kappa_{O_3} = 1.67$ is the ratio of leaf resistance for O_3 to leaf resistance for water vapour. The uptake flux is dependent on the stomatal conductance, which is dependent on the photosynthetic rate in JULES. Given g_l is a linear function of photosynthetic rate (Eq. 13, Cox et al., 1999), from Eq. (29) it follows that

$$g_l = g_p F \quad (32)$$

657

where g_p is the leaf conductance in the absence of O_3 effects. Through this mechanism the direct effect of O_3 deposition on photosynthesis also leads to a reduction in stomatal conductance. As the O_3 flux itself depends on the stomatal conductance, which in turn depends upon the net rate of photosynthesis (Cox et al., 1999), the model requires a consistent solution for the net photosynthesis, stomatal conductance and the ozone deposition flux. Equations (30–32) produce a quadratic in F which is solved analytically.

Data from field observation (Karlsson et al., 2004; Pleijel et al., 2004) are used to calibrate plant-ozone effects for the five standard PFTs described by JULES (see Sitch et al. (2007) for details of the calibration procedure and Table 3 for parameter values). Sitch et al. (2007) presented “high” and “low” parameterisations for each PFT to represent species sensitive and less sensitive, respectively, to ozone effects. The default parameter values in JULES are the “low” sensitivity values. Threshold values, $F_{O_3 \text{ crit}}$, are taken at 1.6 and $5 \text{ nmol m}^{-2} \text{s}^{-1}$ for the woody and grass PFTs, respectively. Although a threshold of 5 implies a smaller O_3 dose for grasses, the gradient of the dose-response function (a), is larger, and therefore grasses may become more sensitive to ozone exposure than trees at high ozone concentrations. For shrubs we assume the same plant-ozone sensitivity as broad-leaf trees.

3.4 Plant respiration

Plant respiration, R_p , is split into maintenance and growth respiration (Cox et al., 1999):

$$R_p = R_{pm} + R_{pg} \quad (33)$$

Growth respiration is assumed to be a fixed fraction of the net primary productivity, thus:

$$R_{pg} = r_g (\Pi_G - R_{pm}) \quad (34)$$

where Π_G is the gross primary productivity, and the growth respiration coefficient is set to $r_g = 0.25$ for all PFTs. Leaf maintenance respiration is equivalent to the moisture modified canopy dark respiration, βR_{dc} , while root and stem respiration is assumed

658

The temperature of the top soil layer (typically 10 cm deep) is used in both cases. Figure 2 compares these alternative temperature functions.

The effect of soil moisture is described as

$$f_{\theta} = \begin{cases} 1 - 0.8(S - S_o) & \text{for } S > S_o \\ 0.2 + 0.8 \left(\frac{S - S_{\min}}{S_o - S_{\min}} \right) & \text{for } S_{\min} < S \leq S_o \\ 0.2 & \text{for } S \leq S_{\min} \end{cases} \quad (49)$$

- 5 where S and S_o are the unfrozen soil moisture content of the top soil layer and the optimum soil moisture, both expressed as a fraction of saturation. $S_o = 0.5(1 + S_w)$ and $S_{\min} = 1.7S_w$, where S_w is the soil moisture at wilting point. The general form of the moisture function from Cox (2001) has been retained in preference to the RothC moisture function because of its ability to simulate reduced respiration in very wet soils. However, it has been revised (the original set $S_{\min} = S_w$) so as to simulate a greater sensitivity of respiration reduction in dry soils, which gave a better fit to the observed site-level seasonal cycle of respiration. The importance of moisture controls on future soil carbon is discussed in Jones and Falloon (2009).

The effect of vegetation cover is described as

$$15 \quad F_v(v) = 0.6 + 0.4 \cdot (1 - v) \quad (50)$$

varying linearly from 0.6 under fully vegetated soil to 1 under completely bare soil.

The carbon pools are updated according to

$$d(\text{DPM})/dt = \alpha_{\text{dr}} \Lambda_c - R_{\text{DPM}} \quad (51)$$

$$d(\text{RPM})/dt = (1 - \alpha_{\text{dr}}) \Lambda_c - R_{\text{RPM}} \quad (52)$$

$$20 \quad d(\text{BIO})/dt = 0.46 \cdot \beta R_s - R_{\text{BIO}} \quad (53)$$

$$d(\text{HUM})/dt = 0.54 \cdot \beta R_s - R_{\text{HUM}} \quad (54)$$

where R_s is the total respiration rate, summed over the 4 pools, the final R_i terms are respiration rates for each pool, and α_{dr} controls the ratio of litter input to DPM

663

and RPM, taking values of 0.25 for trees, 0.33 for shrubs, 0.67 for natural grass and 1.44 for crops. β depends on soil texture to account for the protective effect of small particle sizes. Carbon from decomposition of all 4 carbon pools is partly released to the atmosphere and partly feeds the BIO and HUM pools.

- 5 It is expected that the inclusion of multi-pool dynamics in the soil carbon model will dampen the transient response of soil carbon storage to both changes in litter input and changes in climate (Jones et al., 2005), although the long-term sensitivity will be unchanged if the same Q_{10} function of sensitivity to temperature is used.

5.2 Methane emissions from wetlands

- 10 The methane emission from the wetland fraction of each gridbox is calculated following Gedney et al. (2004) as:

$$F_{\text{CH}_4} = f_{\text{wet}} k_{\text{CH}_4} C_{\text{eff}} Q_{10-\text{CH}_4}^{0.1(T_{\text{soil}} - T_0)} \quad (55)$$

- 15 where k_{CH_4} is a global constant, C_{eff} is the effective substrate availability, $Q_{10-\text{CH}_4}$ is a temperature-dependent Q_{10} factor and T_0 is a reference temperature. f_{wet} is the fraction of the gridbox that is considered to be wetland (i.e. stagnant water) and is calculated using subgrid topographic information, as described in Part 1. The effective Q_{10} value is calculated as

$$Q_{10-\text{CH}_4}(T) = Q_{10-\text{CH}_4}(T_0)^{T_0/T} \quad (56)$$

- 20 When the four-pool soil carbon model is used the substrate availability is calculated by weighting the size of each pool by its specific respiration rate, otherwise $C_{\text{eff}} = C_s$. The default parameter values are $k_{\text{CH}_4} = 7.4 \times 10^{-12} \text{ kg m}^{-2} \text{ s}^{-1}$, $T_0 = 273.15 \text{ K}$ and $Q_{10-\text{CH}_4}(T_0) = 3.7$.

- photosynthesis, and stomatal conductance, *J. Climate*, **17**, 2281–2299, 2004. 652
- de Pury, D. G. G. and Farquhar, G. D.: Simple scaling of photosynthesis from leaves to canopies without the errors of big-leaf, *Plant Cell Environ.*, **20**, 537–557, 1997. 654
- Enquist, B., Brown, J., and West, G.: Allometric scaling of plant energetics and population density, *Nature*, **395**, 163–166, 1998. 667
- 5 Essery, R., Best, M., and Cox, P.: MOSES 2.2 Technical Documentation, Hadley Centre Technical Note 30, Hadley Centre, Met Office, Bracknell, UK, 2001. 651
- Essery, R. L. H., Best, M. J., Betts, R. A., Cox, P. M., and Taylor, C. M.: Explicit representation of subgrid heterogeneity in a GCM land surface scheme, *J. Hydrometeorol.*, **4**, 530–543, 2003. 643
- 10 Fisher, J. B., Sitch, S., Malhi, Y., Fisher, R. A., Huntingford, C., and Tan, S.-Y.: Carbon cost of plant nitrogen acquisition: A mechanistic, globally applicable model of plant nitrogen uptake, retranslocation, and fixation, *Global Biogeochem. Cy.*, **24**, doi:10.1029/2009GB003621, 2010a. 670
- 15 Fisher, R., McDowell, N., Purves, D., Moorcroft, P., Sitch, S., Cox, P., Huntingford, C., Meir, P., and Woodward, F. I.: Assessing uncertainties in a second-generation dynamic vegetation model caused by ecological scale limitations, *New Phytol.*, **187**, 666–681, doi:10.1111/j.1469-8137.2010.03340.x, 2010b. 670
- 20 Friedlingstein, P., Cox, P. M., Betts, R. A., Bopp, L., von Bloh, W., Brovkin, V., Cadule, P., Doney, S., Eby, M., Fung, I., Bala, G., John, J., Jones, C. D., Joos, F., Kato, T., Kawamiya, M., Knorr, W., Lindsay, K., Matthews, H. D., Raddatz, T., Rayner, P., Reick, C., Roeckner, E., Schnitzler, K. G., Schnur, R., Strassmann, K., Weaver, A. J., Yoshikawa, C., and Zeng, N.: Climate–carbon cycle feedback analysis, results from the C4MIP model intercomparison, *J. Climate*, **19**, 3337–3353, doi:10.1175/JCLI3800.1, 2006. 643
- 25 Friend, A. D., Shugart, H. H., and Running, S. W.: A physiology-based model of forest dynamics, *Ecology*, **74**, 792–797, 1993. 659, 668
- Gedney, N., Cox, P. M., and Huntingford, C.: Climate feedback from wetland methane emissions, *Geophys. Res. Lett.*, **31**, L20503, doi:10.1029/2004GL020919, 2004. 644, 664
- Hoefnagel, M. H. N., Atkin, O. K., and Wiskich, J. T.: Interdependence between chloroplasts and mitochondria in the light and the dark, *Bba-Bioenergetics*, **1366**, 235–255, 1998. 655
- 30 Huntingford, C., Booth, B. B. B., Sitch, S., Gedney, N., Lowe, J. A., Liddicoat, S. K., Mercado, L. M., Best, M. J., Weedon, G. P., Fisher, R. A., Lomas, M. R., Good, P., Zelazowski, P., Everitt, A. C., Spessa, A. C., and Jones, C. D.: IMOGEN: an intermediate complexity

673

- model to evaluate terrestrial impacts of a changing climate, *Geosci. Model Dev.*, **3**, 679–687, doi:10.5194/gmd-3-679-2010, 2010. 670
- Jacobs, C.: Direct impact of atmospheric CO₂ enrichment on regional transpiration, Ph.D. thesis, Wageningen Agricultural University, 1994. 649
- 5 Jenkinson, D. S.: The turnover of organic-carbon and nitrogen in soil, *Philos. T. R. Soc. Lond.*, **329**, 361–368, 1990. 644, 662, 687
- Jogireddy, V., Cox, P. M., Huntingford, C., Harding, R. J., and M., M. L.: An improved description of canopy light interception for use in a GCM land-surface scheme: calibration and testing against carbon fluxes at a coniferous forest, Hadley Centre Technical Note 63, Hadley Centre, Met Office, Exeter, UK, 2006. 652, 655
- 10 Jones, C. D. and Falloon, P. D.: Sources of uncertainty in global modelling of future soil organic carbon storage, in: *Uncertainties in Environmental Modelling and Consequences for Policy Making*. NATO Science for Peace and Security Series, edited by: Baveye, P., Mysiak, J., and Laba, M., Springer, Dordrecht, Netherlands, 283–315, 2009. 663
- 15 Jones, C. D., Cox, P. M., Essery, R. L. H., Roberts, D. L., and Woodage, M. J.: Strong carbon cycle feedbacks in a climate model with interactive CO₂ and sulphate aerosols, *Geophys. Res. Lett.*, **30**, doi:10.1029/2003GL016867, 2003. 644
- Jones, C. D., McConnell, C., Coleman, K. W., Cox, P., Falloon, P. D., Jenkinson, D., and Powlson, D.: Global climate change and soil carbon stocks; predictions from two contrasting models for the turnover of organic carbon in soil, *Glob. Change Biol.*, **11**, 154–166, doi:10.1111/j.1365-2486.2004.00885.x, 2005. 644, 664
- 20 Jones, C. D., Cox, P. M., and Huntingford, C.: Climate-carbon cycle feedbacks under stabilization, *Tellus A*, **58B**, doi:10.1111/j.1600-0889.2006.00217.x, 2006. 643
- Karlsson, P. E., Uddling, J., Braun, S., Broadmeadow, M., Elvira, S., Gimeno, B. S., Le Thiec, D., Oksanen, E., Vandermeiren, K., Wilkinson, M., and Emberson, L.: New critical levels for ozone effects on young trees based on AOT40 and simulated cumulative leaf uptake of ozone, *Atmos. Environ.*, **38**, 2283–2294, 2004. 658
- 25 Knohl, A., Schulze, E. D., Kolle, O., and Buchmann, N.: Large carbon uptake by an unmanaged 250-year-old deciduous forest in Central Germany, *Agr. Forest Meteorol.*, **118**, 151–167, 2003. 656
- 30 Le Quéré, C., Raupach, M. R., Canadell, J. G., Marland, G., Bopp, L., Ciais, P., Conway, T. J., Doney, S. C., Feely, R. A., Foster, P., Friedlingstein, P., Gurney, K., Houghton, R. A., House, J. I., Huntingford, C., Levy, P. E., Lomas, M. R., Majkut, J., Metzler, N., Ometto, J. P., Peters,

674

- G. P., Prentice, I. C., Randerson, J. T., Running, S. W., Sarmiento, J. L., Schuster, U., Sitch, S., Takahashi, T., Viovy, N., van der Werf, G. R., and Woodward, F. I.: Trends in the sources and sinks of carbon dioxide, *Nature Geosci.*, 2, 831–836, 2009. 642
- Leuning, R.: A critical appraisal of a combined stomatal-photosynthesis model for C₃ plants, *Plant Cell Environ.*, 18, 357–364, 1995. 649
- Lloyd, J., Grace, J., Miranda, A. C., Meir, P., Wong, S. C., Miranda, B. S., Wright, I. R., Gash, J. H. C., and McIntyre, J.: A Simple Calibrated Model of Amazon Rain-Forest Productivity Based on Leaf Biochemical-Properties, *Plant, Cell Environ.*, 18, 1129–1145, 1995. 654
- McGuire, A. D., Sitch, S. A., Clein, J. S., Dargaville, R., Esser, G., Foley, J., Heimann, M., Joos, F., Kaplan, J. O., Kicklighter, D. W., Meier, R. A., Moore-III, B., Prentice, I. C., Ramankutty, N., Reichenau, T., Schloss, A., Tian, H., Williams, L. J., and Wittenberg, U.: Carbon Balance of the Terrestrial Biosphere in the Twentieth Century: Analyses of CO₂, Climate and Land Use Effects With Four Process-Based Ecosystem Models, *Global Biogeochem. Cy.*, 15, 183–206, 2001. 642
- Meir, P., Kruijt, B., Broadmeadow, M., Barbosa, E., Kull, O., Carswell, F., Nobre, A., and Jarvis, P. G.: Acclimation of photosynthetic capacity to irradiance in tree canopies in relation to leaf nitrogen concentration and leaf mass per unit area, *Plant Cell Environ.*, 25, 343–357, 2002. 655
- Mercado, L. M., Huntingford, C., Gash, J. H. C., Cox, P. M., and Jogireddy, V.: Improving the representation of radiation interception and photosynthesis for climate model applications, *Tellus B*, 59, 553–565, 2007. 654, 655
- Mercado, L. M., Bellouin, N., Sitch, S., Boucher, O., Huntingford, C., M., W., and Cox, P. M.: Impact of Changes in Diffuse Radiation on the Global Land Carbon Sink, *Nature*, 458, 1014–1018, 2009. 644, 652, 656
- Monsi, M. and Saeki, T.: Ueber den Lichtfaktor in den Pflanzengesellschaften und seine Bedeutung fuer die Stoffproduktion, *Jap. J. Bot.*, 14, 22–52, 1953. 650
- Pacifico, F., Harrison, S. P., Jones, C. D., Arneth, A., Sitch, S., Weedon, G. P., Barkley, M. P., Palmer, P. I., Serça, D., Potosnak, M., Fu, T. M., Goldstein, A., Bai, J., and Schurgers, G.: Evaluation of a photosynthesis-based biogenic isoprene emission scheme in JULES and simulation of isoprene emissions under modern climate conditions, *Atmos. Chem. Phys. Discuss.*, 10, 28311–28354, doi:10.5194/acpd-10-28311-2010, 2010. 670
- Phillips, O. L., Aragao, L. E. O. C., Lewis, S. L., Fisher, J. B., Lloyd, J., Lopez-Gonzalez, G., Malhi, Y., Monteagudo, A., Peacock, J., Quesada, C. A., van der Heijden, G., Almeida, S.,

- Amaral, I., Arroyo, L., Aymard, G., Baker, T. R., Banki, O., Blanc, L., Bonal, D., Brando, P., Chave, J., Alves de Oliveira, A. C., Cardozo, N. D., Czimczik, C. I., Feldpausch, T. R., Freitas, M. A., Gloor, E., Higuchi, N., Jimenez, E., Lloyd, G., Meir, P., Mendoza, C., Morel, A., Neill, D. A., Nepstad, D., Patino, S., Cristina Penuela, M., Prieto, A., Ramirez, F., Schwarz, M., Silva, J., Silveira, M., Thomas, A. S., ter Steege, H., Stropp, J., Vasquez, R., Zelazowski, P., Alvarez Davila, E., Andelman, S., Andrade, A., Chao, K.-J., Erwin, T., Di Fiore, A., Honorio C, E., Keeling, H., Killeen, T. J., Laurance, W. F., Pena Cruz, A., Pitman, N. C. A., Nunez Vargas, P., Ramirez-Angulo, H., Rudas, A., Salamao, R., Silva, N., Terborgh, J., and Torres-Lezama, A.: Drought sensitivity of the Amazon rainforest, *Science*, 323, 1344–1347, doi:10.1126/science.1164033, 2009. 642
- Pleijel, H., Danielsson, H., Ojanperä, K., De Temmerman, L., Högy, P., Badiani, M., and Karlsson, P. E.: Relationships between ozone exposure and yield loss in European wheat and potato- a comparison of concentration- and flux-based exposure indices, *Atmos. Environ.*, 38, 2259–2269, 2004. 657, 658
- Prentice, I. C., Farquhar, G. D., Fasham, M. J. R., Goulden, M. L., Heimann, M., Jaramillo, V. J., Kheshgi, H. S., Le Quéré, C., Scholes, R. J., and Wallace, D. W. R.: Dynamic Global Vegetation Modeling: Quantifying Terrestrial Ecosystem Responses to Large-Scale Environmental Change, in: *Climate Change 2001: The Scientific Basis. Contribution of Working Group I to the Third Assessment Report of the Intergovernmental Panel on Climate Change*, edited by Houghton, J. T., Ding, Y., Griggs, D. J., Noguer, M., van der Linden, P. J., Dai, X., Maskell, K., and Johnson, C. A., Cambridge University Press, Cambridge, United Kingdom and New York, NY, USA, 183–237, 2001. 642
- Prentice, I. C., Bondeau, A., Cramer, W., Harrison, S. P., Hickler, T., Lucht, W., Sitch, S., Smith, B., and Sykes, M. T.: Dynamic global vegetation modeling: quantifying terrestrial ecosystem responses to large-scale environmental change, in: *Terrestrial Ecosystems in a Changing World*, edited by: Canadell, J., Pitelka, L., and Pataki, D., IGBP Book Series, Springer, Heidelberg, Germany, 175–192, 2007. 643
- Rebmann, C., Zeri, M., Lasslop, G., Kolle, O., Schulze, E. D., and Feigenwinter, C.: Treatment and assessment of the CO₂-exchange at a complex forest site in Thuringia, Germany, *Agr. Forest Meteorol.*, 150, 684–691, 2010. 656
- Sellers, P., Randall, D., Collatz, C., Berry, J., Field, C., Dazlich, D., Zhang, C., and Collelo, G.: A revised land surface parameterisation (SiB2) for atmospheric GCMs. Part I: Model formulation, *J. Climate*, 9, 676–705, 1996. 647

Table 1. Default values of PFT-specific parameters for leaf biochemistry and photosynthesis.

		Broadleaf tree	Needleleaf tree	C ₃ grass	C ₄ grass	Shrub
k	Extinction coefficient for PAR	0.50	0.50	0.50	0.50	0.50
α (mol CO ₂ [mol PAR photons] ⁻¹)	Quantum efficiency	0.08	0.08	0.12	0.060	0.08
ω	Leaf scattering coefficient for PAR	0.15	0.15	0.15	0.17	0.15
f_d	Dark respiration coefficient	0.015	0.015	0.015	0.025	0.015
r_g	Growth respiration coefficient	0.25	0.25	0.25	0.25	0.25
N_0 (kg N [kg C] ⁻¹)	Top leaf Nitrogen concentration	0.046	0.033	0.073	0.060	0.060
n_{rl}	Ratio of Nitrogen concentrations in roots and leaves	1.00	1.00	1.00	1.00	1.00
n_{sl}	Ratio of Nitrogen concentrations in stem and leaves	0.10	0.10	1.00	1.00	0.10
T_{low} (°C)	Lower temperature parameter	0.0	-10.0	0.0	13.0	0.0
T_{upp} (°C)	Upper temperature parameter	36.0	26.0	36.0	45.0	36.0

Table 2. Summary of options available for the calculation of canopy photosynthesis.

Option	Leaf to canopy scaling	Radiation	N profile	Inhibition of leaf respiration in light
1	Big leaf	Beer's law	Beer's law	no
2	Multi-layer	Two stream	Constant through canopy	no
3	Multi-layer radiation with two layers (sunlit and shaded) for photosynthesis	Two stream	Constant through canopy	no
4	Multi-layer	Two stream	Decreases through canopy	yes
5	Multi-layer including sunlit and shaded leaves in each layer	Two stream with sunfleck penetration	Decreases through canopy	yes

Table 5. Default values of pool-specific parameters for soil carbon. The pools are decomposable and resistant plant material (DPM, RPM), biomass (BIO) and humus (HUM).

		DPM	RPM	BIO	HUM
κ_s (s ⁻¹)	Soil specific respiration rate	3.22×10^{-7}	9.65×10^{-9}	2.12×10^{-8}	6.43×10^{-10}

683

Table 6. Default values of PFT-specific parameters for TRIFFID.

		Broadleaf tree	Needleleaf tree	C ₃ grass	C ₄ grass	Shrub
γ_v (360 days) ⁻¹	Disturbance rate	0.005	0.007	0.20	0.20	0.05
γ_r (360 days) ⁻¹	Turnover rate for root biomass	0.25	0.15	0.25	0.25	0.25
γ_w (360 days) ⁻¹	Turnover rate for woody biomass	0.005	0.005	0.20	0.20	0.05
L_{max}	Maximum LAI	9.00	5.00	4.00	4.00	3.00
L_{min}	Minimum LAI	1.00	1.00	1.00	1.00	1.00

684

Table 7. Default values of PFT-specific parameters for allometry and vegetation carbon.

		Broadleaf tree	Needleleaf tree	C ₃ grass	C ₄ grass	Shrub
a_{wl} (kg C m ⁻²)	Allometric coefficient	0.65	0.65	0.005	0.005	0.10
a_{ws}	Ratio of total to respiring stem carbon	10.00	10.00	1.00	1.00	10.00
b_{wl}	Allometric exponent	1.667	1.667	1.667	1.667	1.667
η_{sl} (kg C m ⁻² per unit LAI)	Live stemwood coefficient	0.01	0.01	0.01	0.01	0.01
σ_l (kg C m ⁻² per unit LAI)	Specific leaf density	0.0375	0.1000	0.0250	0.0500	0.0500

685

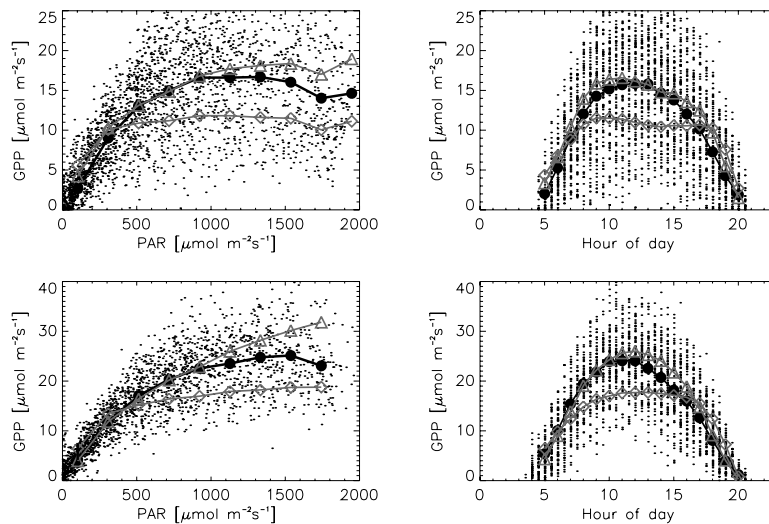


Fig. 1. Evaluation of modelled carbon uptake at a temperate broad leaf (top panel) and needle leaf site (bottom panel). Plots on the left represent the light response of Gross Primary Productivity (GPP) and on the right represent the diurnal cycle of GPP. Lines represent data (closed circles) and model simulations using the big leaf (open rhombus) and multi-layer approaches (open triangles). On the left, both data and simulations are averaged over 200 micromol quanta m⁻² s⁻¹ intervals, and on the right data and simulations are averaged over half hour time periods. In all cases dots represent half-hourly estimated GPP from eddy correlation.

686

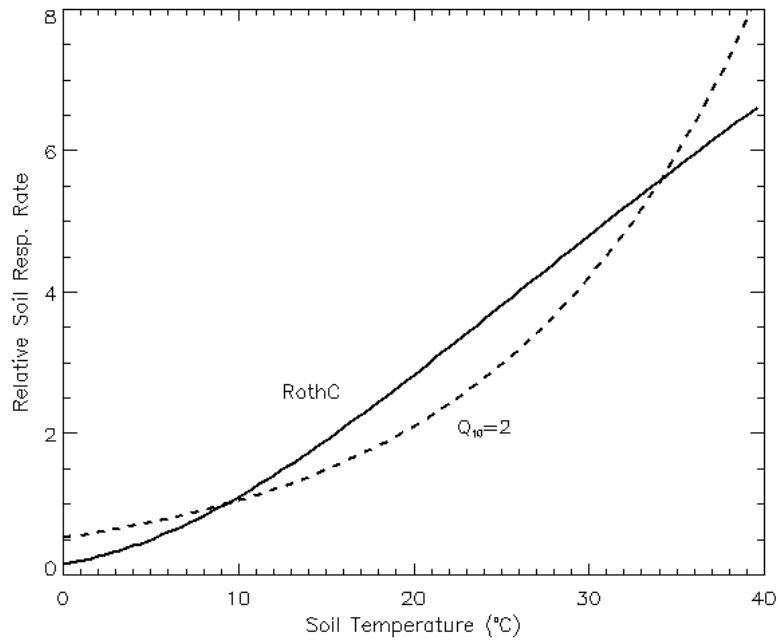


Fig. 2. Comparison of alternative forms for the sensitivity of specific soil respiration to soil temperature in JULES. The dashed line shows a Q_{10} form with $Q_{10} = 2$, the solid line shows the form from the RothC model (Jenkinson, 1990).

687

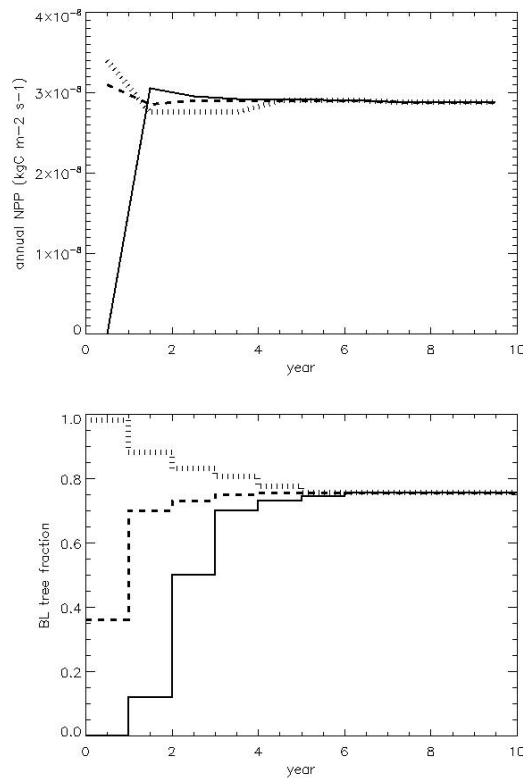


Fig. 3. An example of the spin up of TRIFFID in equilibrium mode. The lines show evolution from different initial conditions with convergence after five calls to TRIFFID. (Top) NPP (Bottom) the fractional coverage of the broadleaf tree type.

688